The combination of rotating disk photocatalytic reactor and TiO$_2$ nanotube arrays for environmental pollutants removal

Aiyong Zhang [a], Minghua Zhou [a,*], Lu Han [a], Qixing Zhou [a,b,**]

[a] Key Laboratory of Pollution Processes and Environmental Criteria of Ministry of Education, College of Environmental Science and Engineering, Nankai University, Tianjin 300071, PR China
[b] Key Laboratory of Terrestrial Ecological Process, Institute of Applied Ecology, Chinese Academy of Sciences, Shenyang 110016, PR China

ABSTRACT

A combined photocatalytic system on one single TiO$_2$-nanotube (TNT)/Ti photocatalyst, which was indeed the functional combination of photon-efficient thin-film and conventional bulk-phase photocatalysis processes, was effectively developed in rotating disk photocatalytic reactor for environmental purification applications. The TNT/Ti rotating disk, of uniform size and well-aligned, was successfully prepared by direct anodic oxidation on a dominantly large surface area of 38 cm^2, compared to the typical 1 cm^2 in available literature. To estimate the potentials of combined photocatalytic system for environmental applications, the degradation of rhodamine B was carried out under the optimized conditions, a substrate removal efficiency of nearly 90% and a mineralization efficiency of 56% were observed for initial 20 mg/L solution after 3 h treatment. Compared with the combined photocatalytic system on TiO$_2$ nanoparticle disk, a significant improvement in substrate removal efficiency of about 25–40% was observed on TNT/Ti disk. It was confirmed that the main degradation of rhodamine B occurred on the upper half of TNT/Ti disk above the heavily colorized sample solution, which was attributed to the superior UV utilization efficiency and the resultant high interfacial photoactivity.

© 2010 Elsevier B.V. All rights reserved.

1. Introduction

The distinguished and attractive performance of TiO$_2$ photocatalysis (PC) has attracted large interests in fields of environmental science and technology due to its high activity, long-term physicochemical stability, non-toxicity and relatively low price [1,2]. However, numbers of problems have also prevented its full industrialization, i.e., light penetration, oxygen transfer, electron–hole recombination and low quantum yield, all of which would lead to a low effectiveness and high cost [3].

To effectively enhance PC performance, several aspects have been systematically investigated, in which the photocatalyst and photoreactor are the two dominant items.

On one hand, the nanoarchitecture of TiO$_2$ photocatalyst plays a critical role in determining the maximum photoconversion efficiency that can be achieved. One-dimensional TiO$_2$ nanotube arrays (1D, TNTs) constitute a material architecture that offers a large internal surface area with lengths sufficient to effectively capture incident illumination in combination with minimal radial dimensions providing facile separation of photogenerated charge. The oriented nature of 1D TNTs makes them excellent electron percolation pathways for charge transfer between interfaces, as well as the excellent optical, electrochemical, photoelectrochemical and photoelectrocatalytic properties.

Moreover, the observed superiorities of 1D TNT/Ti over zero-dimensional TiO$_2$ nanoparticle films (0D TNPs) could be mainly attributed to the following four distinguished advantages [4–11]: (1) the high surface to volume ratio, (2) the convenient way for charge transfer, (3) the high photon-collection efficiency and (4) the large band gap energy.

In addition, the 0D TNPs are inevitably subjected to an irregular arrangement and usually diminish their valid interfacial areas, while the weak bonding structure between TNPs and conductive glass probably inhibits interfacial electron-transfer, which finally affects photoelectric efficiency [12]. In comparison, the 1D TNTs can be directly grown on Ti metal foil through a regularly chemical anodization process. Moreover, these TNT array layers could tightly connect with Ti matrix to form an integrative structure, and show a stronger attachment to parent titanium substrate and a better photoactivity due to the improved electron transport and reduced charge recombination [13].

On the other hand, the photoreactor also plays a very important role in the whole PC process [14,15]. Since the photocatalytic oxidant species, mainly hydroxyl and peroxyl radicals, have very short lifetimes and are very easy to terminate, the PC occurs mainly on the surface and/or in very close proximity of the photocatalyst. Therefore, in this case, pollutants must be first transported to photocatalyst surface, and then photooxidized there. Consequently, the thin-film photoreactor is proposed, in which only a thin liquid film exists between the light source and photocatalyst, so the photon loss through absorption within liquid phase dramatically diminishes. When the light source is fixed, sacrificing only a little UV power to get a large illumination intensity is an effective consideration for photoreactor design [16].

Furthermore, in 2000 and 2002, Dionysiou's group effectively reported a rotating disk photocatalytic reactor (RDPR) for various organics degradation [17,18] and have gained a lot of attentions and insights [12,19–25]. In RDPR, the upper half of rotating disk is exposed to air to perform photo-efficient thin-film PC (TPC), the lower half is immersed in bulk wastewater to perform conventional bulk-phase PC (BPC), both of which together form a combined photocatalytic system (TBPC). Therefore, the RDPR should be recognized as a combined photoreactor of both thin-film and bulk-phase types, and the formed TBPC is anticipated to be powerful since it employs not only photon-efficient TPC but also conventional BPC processes to simultaneously oxidize pollutants in one single treatment system [26].

The RDPR is simple in design, operation and scaling [17], and the major advantages include immobilization of photocatalyst, reaction within a thin liquid film, high illumination efficiency, good stirring, no oxygenating other than oxygen uptake from the surrounding air and operation cost-effectiveness [25–27].

Up to now, the RDPR has been informatively studied on randomly packed 0D TNPs (TNP–TBPC) [12,17–25], some dramatic superiorities are well validated and show great potentials in environmental applications. In this study, we reported a study on RDPR with highly ordered, vertically oriented 1D TNTs to form a novel TBPC system (TNT–TBPC). The 1D TNT/Ti disk was prepared by electrochemical anodization in fluoric electrolyte, with ethylene glycol utilized as organic solvent.

The objective was to introduce a novel TNT–TBPC, of both highly photon- and photocarrier-efficient, on one single 1D TNTs photocatalyst for environmental applications. The effort was to combine the superior photocatalytic system of TBPC with the superior photocatalyst of 1D TNTs in one single PC process for organic pollutants degradation.

However, it should be also pointed out that we have effectively combined the large-area 1D TNT/Ti photocatalyst with the photon-efficient RDPR system in photoelectrocatalysis (PEC) mode [28]. In this work, the following four differences could be obviously recognized: (1) the replacement of PEC with PC due to its operation simplicity and wide usage, (2) the prepared 1D TNT arrays was dramatically longer and the 1D TNT/Ti rotating disk was more photoactive, (3) the introduction of electrochemical and photoelectrochemical characterizations to gain more informative insights into photocatalytic mechanisms and (4) the quantitative comparisons between 0D TNP/Ti and 1D TNT/Ti photocatalytic disks in the combined TBPC system.

2. Experimental

2.1. Materials and reagents

Round titanium sheets (99.6% purity, diameter 70 mm; thickness 0.25 mm, surface area 38 cm^2) were employed for TNT/Ti anodization. Ethylene glycol (EG) and Na$_2$SO$_4$ were employed as

the supporting electrolyte, the preparation of TNP/Ti disk employed commercial TiO$_2$ (P25, Degussa AG, Germany, a mixture of ca. 30% rutile and 70% anatase, a mean size about 25 nm, BET surface area 55 m^2/g). Rhodamine B (RB) and all other chemicals were of analytical reagent grade and used as received. Aqueous solutions were prepared in doubly deionized water.

2.2. TNT/Ti Preparation

TNT/Ti sample was prepared by anodization of the circular titanium foil in an organic supporting electrolyte. The electrolyte was prepared by 0.5 wt.% NH$_4$F in EG containing doubly deionized water with a conductivity of 460 uS/cm (98 vol.% EG + 2 vol.% H$_2$O + 0.5 wt.% NH$_4$F). The electrochemical treatment consisted of a potential ramp from the open-circuit potential to 45 V, followed by holding at 45 V for 6 h, further detailed information was available [28,29].

A field emission scanning electron microscope (FESEM; Hitachi, S-4700) was used to analyze the TNTs formation and morphology. The length and diameter were obtained from SEM cross-sections after scratching through the TNTs with a sharp metallic tip. Diffuse reflectance ultraviolet and visible spectra (UV-DRS) was measured on a UV–vis spectrophotometer (UV-2401 PC, Shimadzu). Fine BaSO$_4$ powder was used as a standard for baseline and the spectra was recorded in a range 200–800 nm. Glancing angle X-ray diffraction (GXRD) was done using a Philips-12045 B/3 diffractometer to identify the sample structure.

2.3. RDPR

The employed PC reactor was 85 mm in diameter, 15 mm in gap thickness and approximately 39 ml in volume (Fig. 1). The container in the RDPR was made of quartz since the 254 nm radiation was utilized. Indeed, the proposed RDPR with 1D TNT/Ti rotating disk could fully realize all the main properties of an effective and energy-efficient PC system [16,30].

2.4. Degradation experiment

A 36 mL RB aqueous solution with different concentrations was used as the target sample, the experiments were all carried out at room temperature. Before PC degradation, the TNT/Ti disk was illuminated under ambient air by UV light for 30 min to clear ubiquitous organic pollutants and then put into RB sample solution under continuous disk stirring. Prior to irradiation, the reaction solution was kept aerating in the dark for 60 min, then UV illumination started.

The photoactivity was evaluated by the absorbance spectra of RB solution recorded with a UV–vis spectrophotometer (UV759, Shanghai Precision & Scientific Instrument Co., Ltd. China) at 563 nm. Chemical oxygen demand (COD) was measured by a commercial detector (HACH, DRB 200, DR/890 Colorimeter, America).

In this study, RB photodegradation was performed in three different systems (Fig. 1(b)):

(1) TPC. The photon-efficient TPC process was on only the upper half of TNT/Ti disk in open air and exposed to UV irradiation (19 cm^2), while the lower half was immersed in the highly colorized bulk-phase sample solution and blocked.
(2) BPC. The conventional BPC process was on only the lower half of TNT/Ti disk immersed in the highly colorized bulk-phase sample solution and exposed to UV irradiation (19 cm^2), while the upper half was in open air and blocked.
(3) TBPC. The combined TBPC process was indeed the functional combination of photon-efficient TPC and conventional BPC processes on the whole TNT/Ti disk exposed to UV irradiation
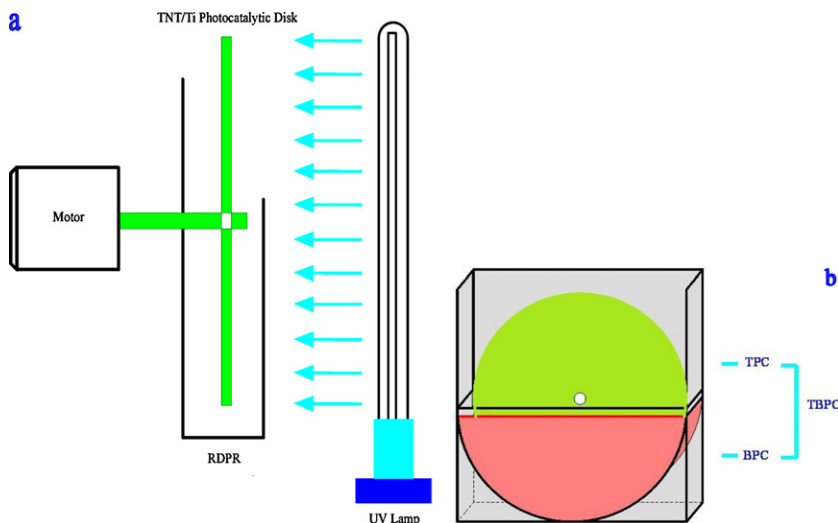
Fig. 1. Schematic diagram (a) and TBPC combined mechanism (b) of the RDPR.

($38\,cm^2$), in which the upper half in open air was exposed to UV irradiation ($19\,cm^2$) and possessed the photon-efficient TPC process, while the lower half immersed in bulk-phase sample solution was exposed to UV irradiation ($19\,cm^2$) and possessed the conventional BPC process.

2.5. Photoelectrochemical measurements

Electrochemical and photoelectrochemical measurements were performed on an electrochemical station (CHI 660D, Shanghai Chenhua Instrument Co. Ltd., China) in a standard three-electrode system, in which the TNT/Ti or TNP/Ti electrode was utilized as the anode, a Pt foil as the cathode and a SCE as the reference electrode. A 15 W low-pressure mercury lamp (TUV 15W G15 T8, Philips Corporation, Holland) was used as the 254 nm radiation, and the supporting electrolyte was 0.01 M Na_2SO_4 aqueous solution. In addition, a functional combination of photolytic (direct photolysis) and photocatalytic phenomena might occur in this study due to the utilized 254 nm radiation.

3. Results and discussion

3.1. TNT/Ti disk

According to some recent studies [31–34], nanotube (NTs) formation in fluoric electrolytes occurs as a result of the interplay among three simultaneous processes: the field-assisted oxidation of Ti to form TiO_2, the field-assisted dissolution of Ti metal ions in electrolyte at the metal/oxide interface and the chemical dissolution of Ti and TiO_2 at the oxide/electrolyte interface due to etching by fluoride ions, which is substantially enhanced by the presence of H$^+$ ions.

However, producing 1D TNT arrays on relatively large surface area detrimentally involves the formation of TNTs bundle layer in anodic film [8], which would lead to films cracking due to the relatively high surface tension force of the electrolyte liquid and capillary force of the liquid acting between the adjacent NTs [34,35]. Such capillary forces have the potentials to cause not only bundling/clustering of NTs but also cracks/curls in the film, depending on, for instance, the surface tension of the liquid and the NT stiffness, aspect ratio, density and wall thickness [8,10,29,36,37].

The obtained NTs were 14.9 μm long with an average pore size of 75 nm and a wall thickness of 17 nm (Fig. 2(a) and (b)), with

the dominant tubular nanostructure (Fig. 2(c) and (d)). Obviously, although the length of NTs and the thickness of 1D TNT/Ti arrays were both significantly larger, the morphological quality was lower than the previous work [28].

As indicated in Fig. 2(e), the nanotubular film was effectively crystallized to UV photoactive anatase phase upon high-temperature thermal annealing due to the increased conductivity of the layer by minimizing the structural defects that act as electron traps [38].

X-ray photoelectron spectra (XPS) analyses (Fig. 2(f), (g) and (h)) evidenced the dominant formation of TiO_2, these findings were consistent with the XRD analysis (Fig. 2(e)). UV-DRS analysis indicated the strong absorption of UV light of 200–400 nm, which significantly validated the utilization of 254 nm radiation in this work.

3.2. TNT–TBPC system

3.2.1. Combined potentials

The theoretical basis of TNT–TBPC system with the vertically ordered, upright oriented 1D TNT/Ti disk has been similarly reported elsewhere [28].

For RDPR, the most important operation parameter is rotating speed of the photocatalytic disk [12,16–26]. Rotation speed is related to the thickness of carried liquid film on rotating disk as well as the mass transfer coefficients of substrates, intermediates and final products, all of which have significant influences on the PC process.

The thickness of carried liquid film on rotating disk is a crucial factor for TBPC system, and it is determined by both rotation speed and disk diameter. However, in TNT–TBPC, the transition point from laminar to turbular flow would occur more gradually at lower rotating angular velocities and Reynolds numbers due to the high roughness of 1D TNT/Ti rotating disk, compared to those in TNP–TBPC counterpart with 0D TNP/Ti disk [22]. This probably indicated the proposed TNT–TBPC could obtain relatively higher mass transfer coefficients and degradation efficiencies stemmed from the more intense turbulance at relatively lower disk angular velocities, compared to the conventional TNP–TBPC.

Fig. 3 showed the RB degradation as a function of rotation speed of TNT/Ti disk. Changes in rotation speed substantially altered a number of mass transfer characteristics. For example, the turbulence in bulk solution increased with higher rotation speeds, as the mixing in the entrained film [22]. Both of these effects could

effectively improve the external liquid-to-solid mass transfer of the liquid-phase reagent.

When the rotation speed was smaller than a specific value (probably between 20 and 30 rpm in this study, see Fig. 3), the carrying water film was too thin to provide organics to the photocatalytic surface at a rate that was equal to or larger than the degradation capacity of TNT/Ti photocatalytic disk. This detrimental phenomenon could be obviously observed at 5, 10 and 20 rpm, which probably indicated that to maintain a sufficient

water film thickness on TNT/Ti disk was of great importance for the TBPC.

Moreover, at low disk angular velocities (i.e. $\omega < 20$ rpm), the reaction rates were lower due to smaller mass transfer coefficients (which resulted in more significant external mass transfer limitations) and longer time available per rotation (which led to higher down-flow of the liquid film as an effect of gravitational forces). The latter could result in reduced presence of the liquid film in the upper sections of TNT/Ti photocatalytic disk and thus reduce overall
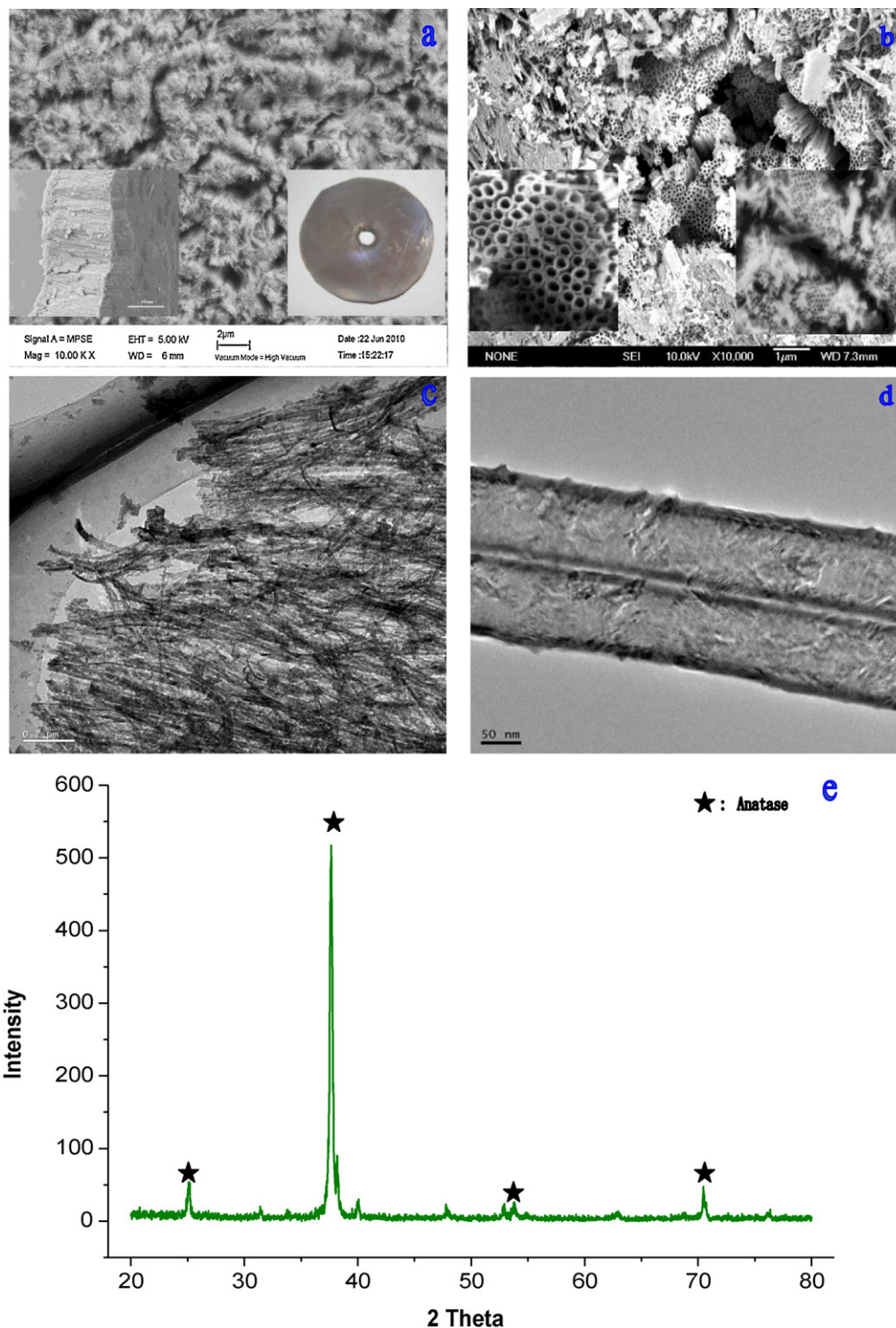

Fig. 2. The typical SEM and TEM (c, d) images, XRD pattern (e) and XPS spectras (f, g, h) of the TNT/Ti disk after high-temperature calcination without ultrasonic treatment.
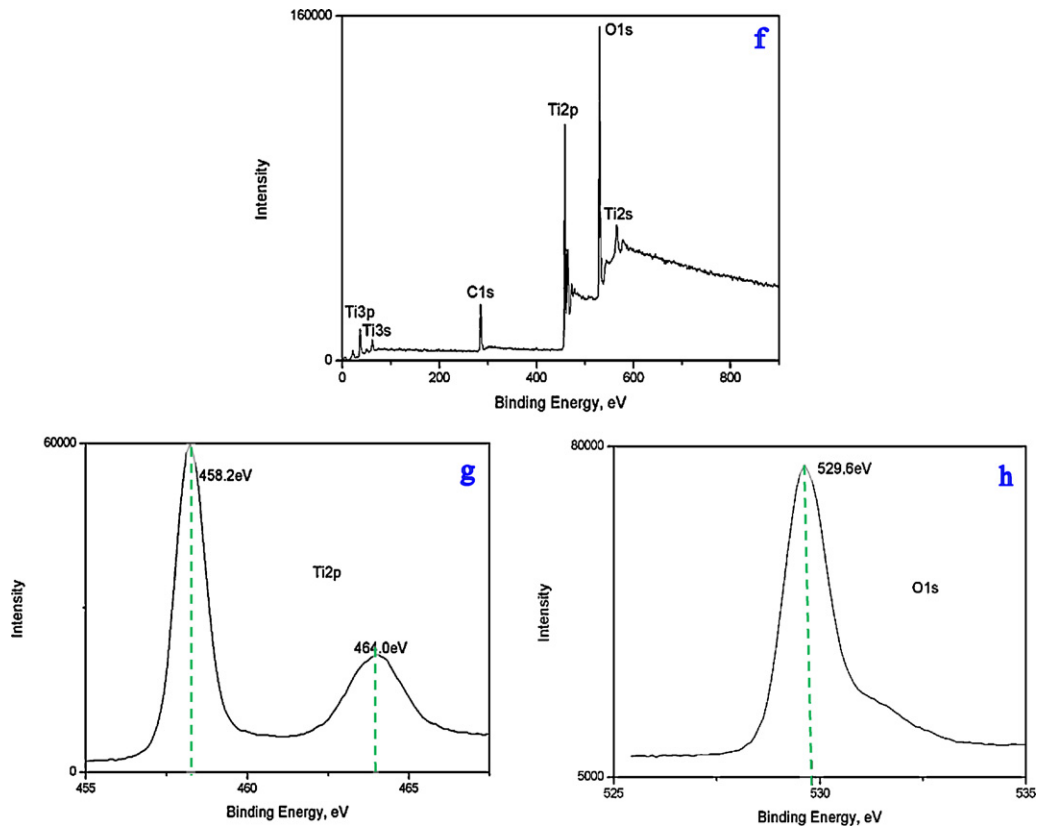
Fig. 2. (*Continued*).

reaction rates, which probably means a mass transfer-limited type of PC process [18], including the mass transfer of substrate and dissolved oxygen from bulk solution to photocatalyst surface as well as degradation intermediates and final products from photocatalyst surface to bulk solution. At 30 rpm, the RB removal efficiency was observed to be considerably improved and reached nearly 90% within 3 h treatment, while no obvious increase was observed when the disk angular velocity further increased. These results probably indicated the TBPC process transferred from mass transfer-limited to surface reaction-limited type, and the carrying water film was sufficiently thick to provide organics to TNT/Ti rotating disk, at a
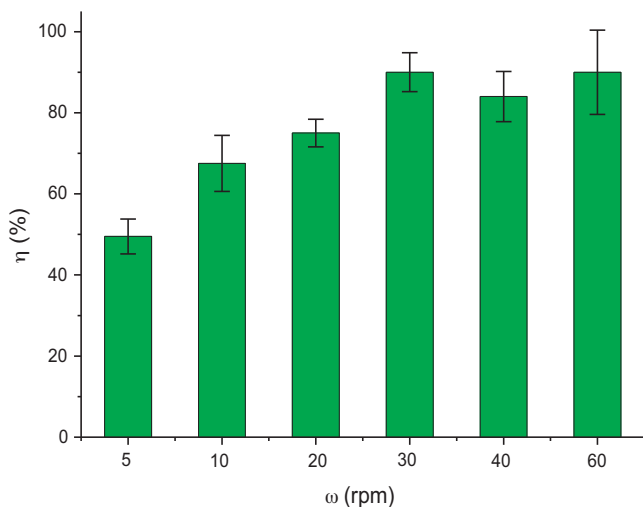
rate which was equal to or larger than the degradation capacity. Consequently, 30 rpm was selected for the following studies.

Fig. 4 indicated the RB degradation in TNT–TBPC system followed quasi-first-order-type kinetics, as evidenced by the linear plots of $\ln(C_0/C)$ versus reaction time, t, in min. Here, C_0 was the initial concentration, and C was the concentration at time t. As illustrated, a removal efficiency of nearly 90% was obtained within 3 h treatment, with an effective COD removal efficiency of 56%. The enhanced photocatalytic activity mainly resulted from the superior photon efficiency, quantum yield and photocarriers separation, transfer and utilization in vertically ordered, upright oriented 1D TNT/Ti disk.

Moreover, although the morphological quality was lower than that of the previous work [28], the photoactivity of the new 14.9 μm 1D TNT/Ti arrays was found to be much higher for RB removal (Fig. 4(b) and (c)). For the previous 11.4 μm 1D TNT/Ti arrays [28], only a RB removal efficiency of about 50% and a marginal COD removal efficiency of 16.8% were obtained within 3 h treatment, respectively. Obviously, this superior photoactivity, which might be mainly attributed to both larger length of NTs and thickness of 1D TNT/Ti disk, could be explained that the amounts of both photons absorption and RB adsorption increased with the thickness of 1D TNT/Ti film, both of which were beneficial to achieving greater photocatalytic degradation and mineralization rates [6].

3.2.2. Combined properties

To explore the combined properties, RB degradation were comparatively investigated in TPC and BPC systems, respectively, and both overall and unit removal efficiencies were calculated. To individually perform TPC and BPC systems in one single RDPR, the two different halves of 1D TNT/Ti photocatalytic disk (upper or lower) were exclusively covered by an UV-resistant opaque plate with suitable size, leaving only the other half exposed to UV irradiation.
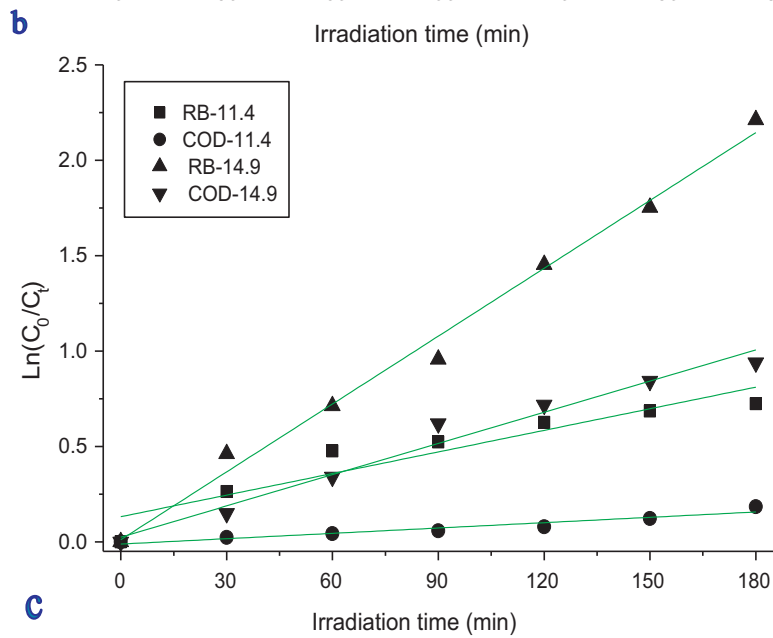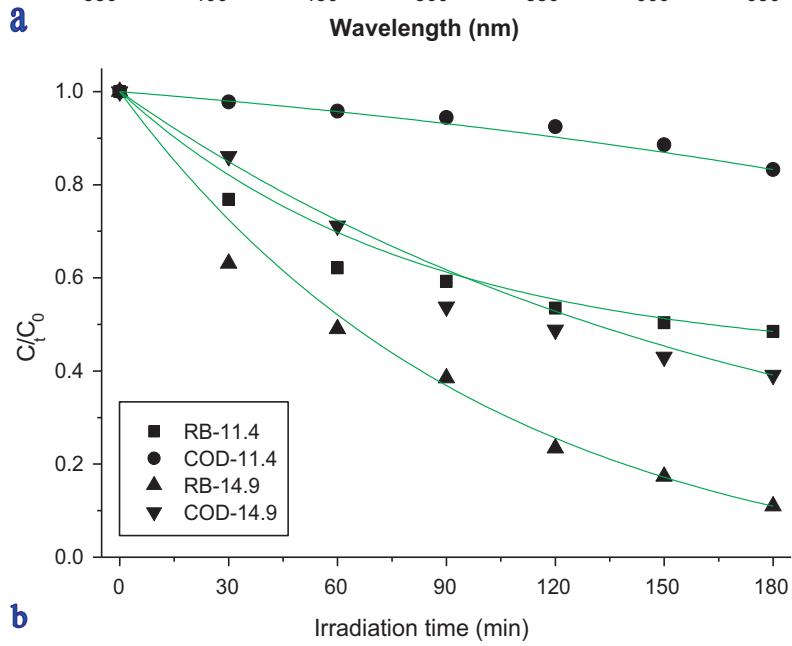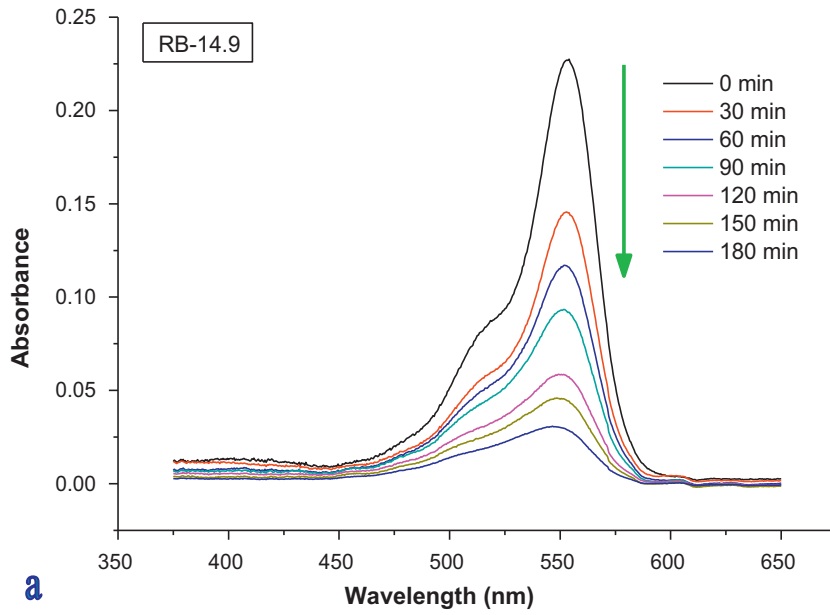

Fig. 3. Effects of rotating velocity (ω) on the TBPC performance for 20 mg/L RB solution.

Fig. 4. TBPC performance under the optimized conditions for 20 mg/L RB solution.
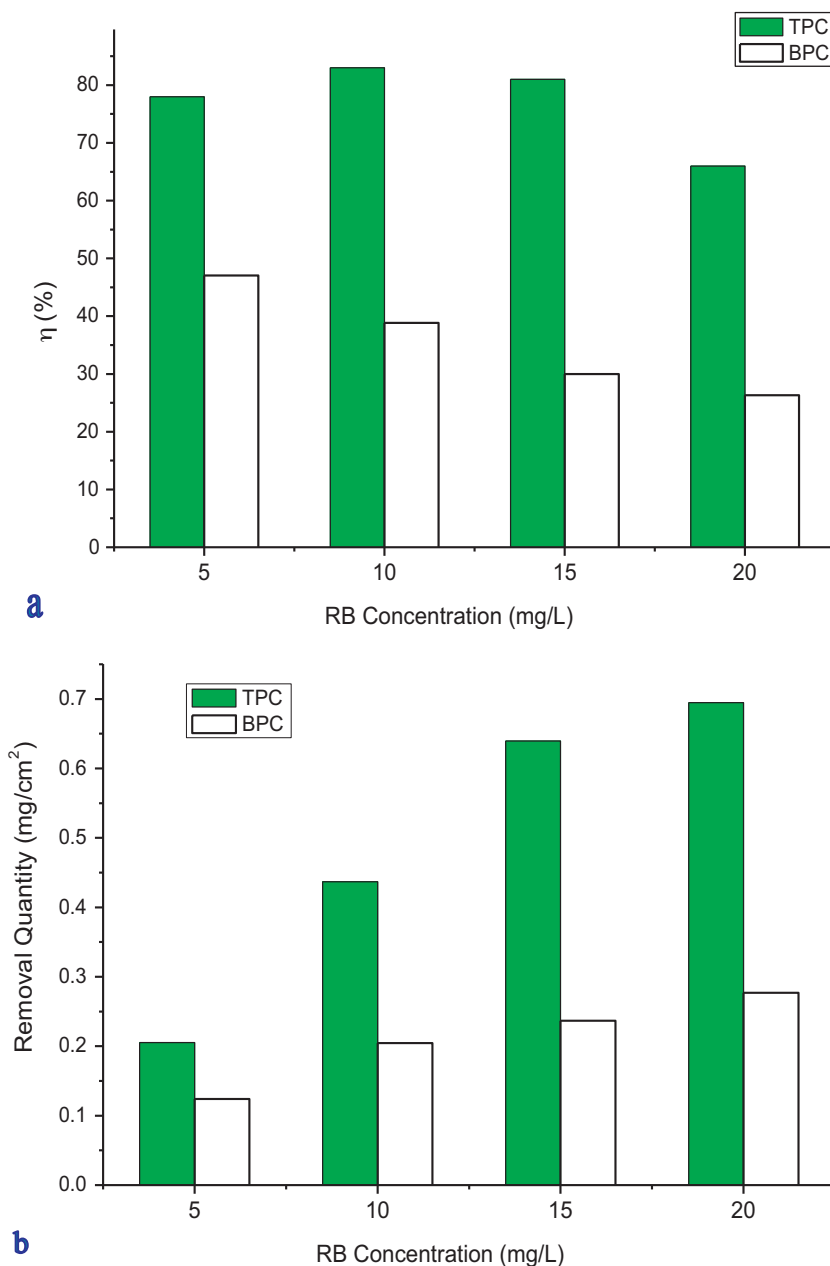
Fig. 5. TPC and BPC performances for RB degradation at ω of 30 rpm.

In principle, the conventional BPC on the lower half of TNT/Ti disk, which was immersed in highly colorized RB solution and exposed to UV irradiation (approximately 19 cm^2), was much less photoactive and consequently exhibited lower RB removal efficiencies, compared to the photon-efficient TPC on the upper half. This ineffectiveness should be mainly attributed to the disadvantageous UV application mode, in which the irradiator was completely blocked by bulk phase RB solution of highly concentrated and colorized, while the quantum yield and oxidation capability were directly related to illumination intensity.

In comparison, in photon-efficient TPC on the upper half of TNT/Ti disk, there was only a thin liquid film between the UV source and photocatalytic disk, therefore, the invalid photon loss within RB filling solution significantly diminished or was even negligible. For the given low-intensity light source in this study, the TPC sacrificed only a little UV intensity to get a high illumination intensity and was proved to be an effective consideration for photoreactor design, with good photon efficiency and photo-driven capacity for environmental applications [12,16–30].

Moreover, the RB removal efficiencies in BPC were observed to be much lower (approximately 30–55%) than those in TPC under identical operation conditions for the solution at various concentrations (Fig. 5(a) and Table 1). Furthermore, the absolute quantities of RB removed by each cm^2 TNT disk showed similar trend (Fig. 5(b)).

Since the formed water film on the upper half of TNT/Ti rotating disk is very thin and therefore the UV photons can easily penetrate to photocatalyst surface and O$_2$ in atmosphere can also diffuse rapidly to photocatalyst surface, both of which lead to a rapid production of $^\bullet$OH and $^\bullet$OOH radicals [31]. Mixing of solution is achieved by disk rotation, and the RDPR has mixing characteristics similar to a continuously stirred tank reactor [27].

These observations might be elucidated in terms of the transmittance of highly colorized RB sample solutions filled in RDPR and surrounding the lower half of TNT/Ti disk, where the BPC occurs

Table 1
The kinetic constants in TPC and BPC systems at ω of 30 rpm.

RB concentration (mg/L)	Kinetic constants[a] k_{app} (min^{-1})	Regression coefficients R^2	Kinetic constants[b] k_{app} (min^{-1})	Regression coefficients R^2
5	0.0086	0.9932	0.0032	0.9663
10	0.0102	0.9860	0.0028	0.9091
15	0.0098	0.9746	0.0021	0.9864
20	0.0064	0.9885	0.0017	0.9620

[a] TPC.
[b] BPC.

[26]. According to Beer's law [38], the inlet UV transmittance is directly proportional to the molarity of target solution and the path length between irradiator and photocatalyst. Moreover, nearly no transmittance was observed for RB solutions of 80 and 100 mg L^{-1} (Fig. 6(c)), which meant that the UV radiation was indeed completely absorbed by the highly concentrated and heavily colorized sample solutions [26]. Without UV irradiation, the photo-driven PC actually became an adsorption–desorption process.

From Fig. 5 and Table 1, it clearly indicated the photon-efficient TPC was much superior over conventional BPC in both overall and unit photodegradation performances, especially for those highly concentrated and heavily colorized reaction systems. Consequently, we could infer the photon-efficient TPC should show greater potentials in environmental applications than the conventional BPC, typically in both aqueous and gaseous photon-driven systems. Moreover, in the proposed TNT–TBPC system, the main degradation and mineralization processes should occur on the upper half of 1D TNT/Ti rotating disk in TPC form, whose effectiveness dominantly determined the total degradation efficiency of PC process.

3.2.3. Combined disks

To estimate the effects of 1D TNT/Ti photocatalytic disk on TBPC system for environmental applications, RB degradation were comparatively carried out on both 1D TNT/Ti (TNT–TBPC) and 0D TNP/Ti (TNP–TBPC) disks with similar thickness, respectively. The 0D TNP/Ti photocatalytic disk was prepared by spreading a viscous dispersion of colloidal TNPs on a conducting circular Ti metal support, as employed in 1D TNT/Ti disk [28].

Generally, compared to randomly packed 0D TNP/Ti disk, the vertically ordered 1D TNT/Ti counterpart that directly grown on Ti metal substrate could result in an obviously large effective surface area, which was in close proximity with the treated sample solutions [5]. Furthermore, the 1D nanotubular photocatalyst could enable diffusive transport of photogenerated holes to oxidizable species more quickly and efficiently, which was realized by minimizing the invalid recombination/loss of photocarriers during the separation and transfer processes [8,9], then the 1D TNT/Ti disk would allow for more efficient UV absorption, decreased bulk recombination and high quantum yield [11].

As a result, for the depicted photo-efficient TBPC system, the incorporation of photocarrier-efficient 1D TNT/Ti photocatalyst would dominantly guarantee the high separation, transfer and utilization efficiencies of photogenerated electro–hole pairs (photocarriers) as well as the resultant distinguished photocatalytic capability by diminishing the invalid recombination/loss of highly active photocarriers. This advantage indicated the attractive photochemical and photocatalytic properties and eventually benefited the highly efficient TNT–TBPC.

Moreover, based on the functional combination as depicted, the proposed TNT–TBPC system on highly ordered, vertically oriented 1D TNT/Ti photocatalytic disk could be accordingly anticipated to possess excellent optical, photochemical and photocatalytic properties for environmental applications, all of which could explain the
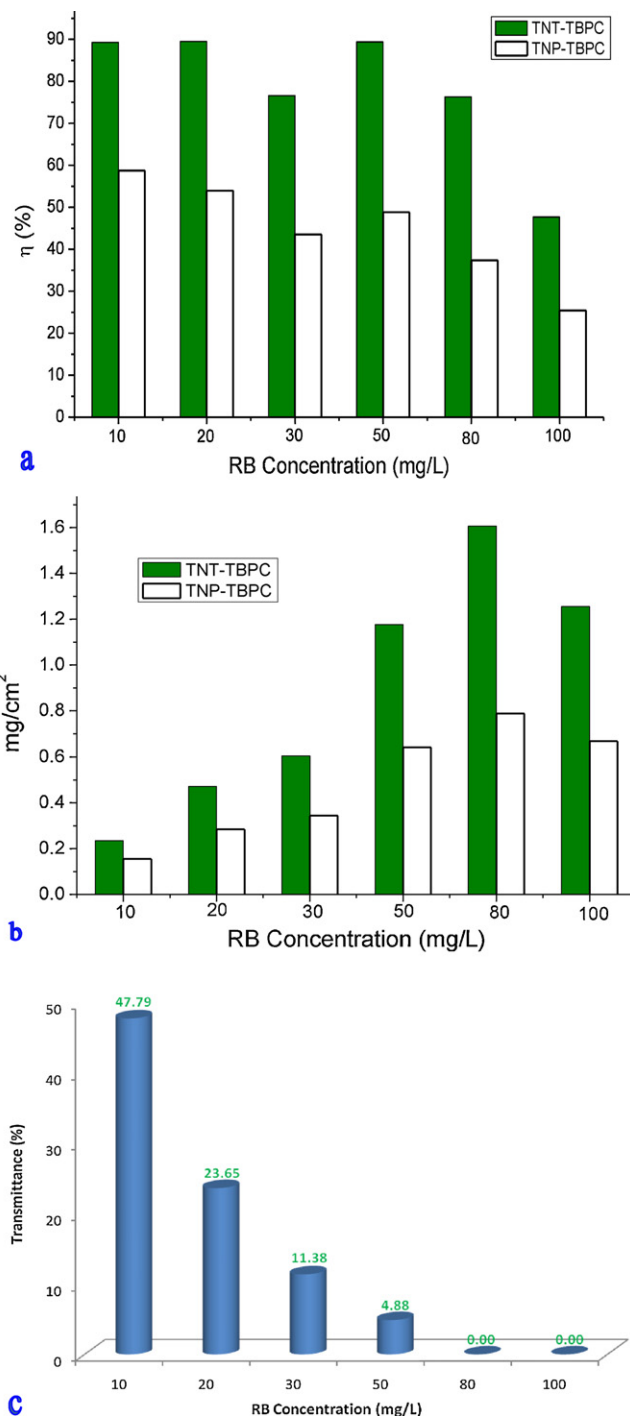
Fig. 6. Total (a) and unit (b) degradation performances of TNP–TBPC and TNT–TBPC at ω of 30 rpm and UV transmittance (c) at 254 nm in 1 cm optical path length for RB solutions.

enhanced RB removal efficiencies of approximately 25–40% on 1D TNT/Ti disk (Fig. 6 and Table 2). Moreover, this enhancement should be mainly attributed to the high surface to volume ratio, stronger internal light-scattering effects and convenient way for photogenerated electrons to transfer to the conductive Ti metal substrate, all of which could dramatically improve the photocatalytic activity and efficiency [4,10].

In principle, the responsive photocurrent intensity could reflect the overall photoelectron-conversion process, a higher photocurrent response means a lower electron-hole recombination and a higher photoelectron transfer efficiency on the highly ordered,
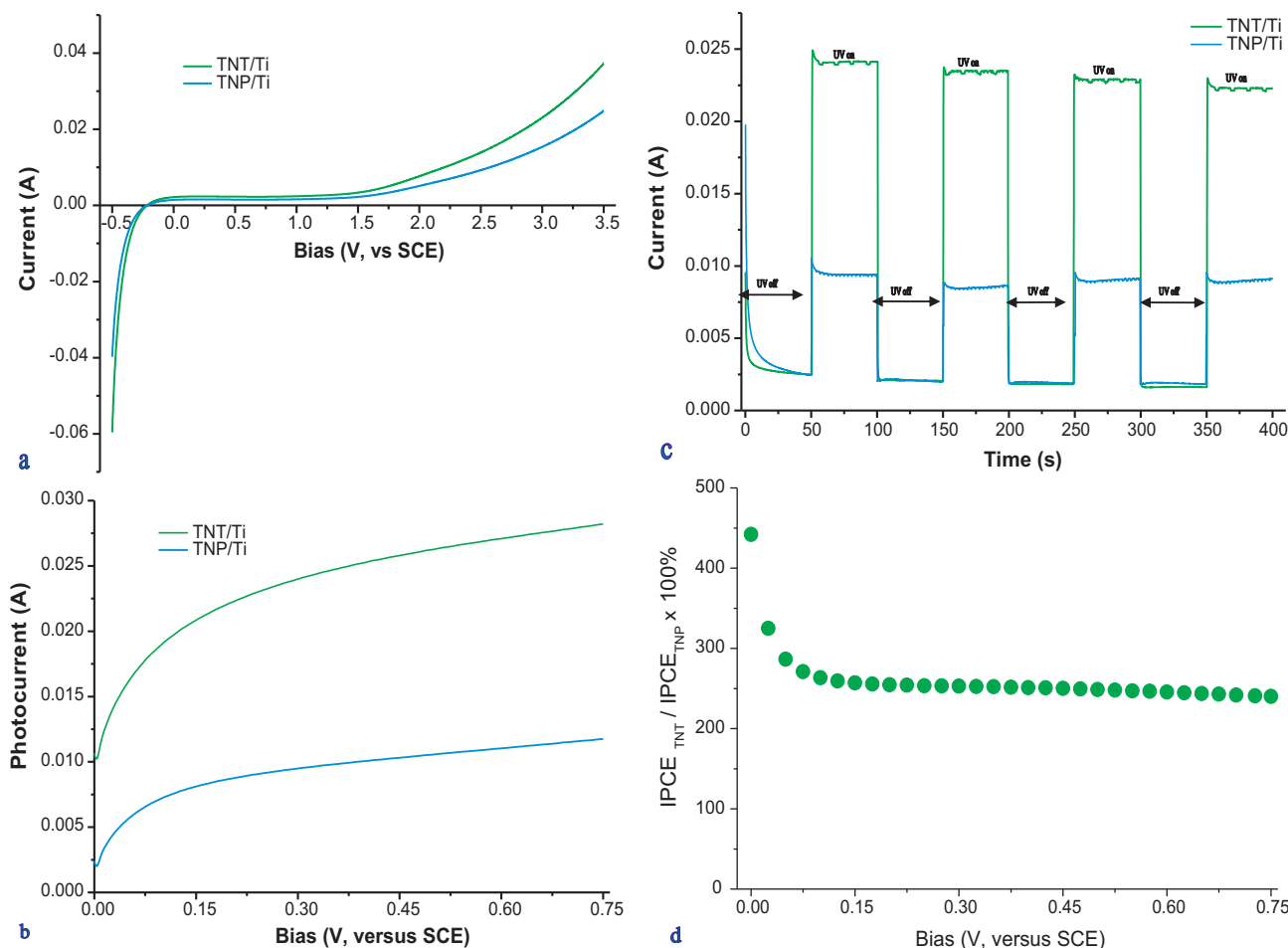
Fig. 7. I–V characteristic curve in dark (a), photocurrent intensity under UV irradiation (b), short-circuit photocurrent intensity at 0.45 V (vs. SCE) (c) and IPCE ratio versus applied potential (vs. SCE) (d) for the 1D TNT/Ti and 0D TNP/Ti disks, respectively.

vertically oriented 1D TNT/Ti photocatalytic disk (Fig. 7(a)–(d)). The measured I–V curves of the two TiO_2 semiconductor/metal junctions at the interface both showed the typical characteristic asymmetric behavior of a typical n-type semiconductor/metal Schottky barrier diode, and the contact resistance of these two photocatalytic disks varied greatly with the direction of external applied electric field, which indicated a strong intrinsic nanoscale effect [4,39] (Fig. 7(a) and (b)).

Moreover, this asymmetric behavior would also serve to enhance the photocatalytic properties of these two rotating disks by directly driving photogenerated electrons from the TiO_2 semiconductor to the conductive Ti metal substrate, which was mainly based on the principle of establishing Schottky barrier with an

electrostatic potential gradient or space charge region, and it consequently expedited the effective separation of photogenerated electron/hole pairs and minimized the invalid recombination of highly active photocarriers. Therefore, the measured short-circuit photocurrent on 1D TNT/Ti disk were much higher than those on 0D TNP/Ti counterpart (Fig. 7 (c)), and the measured incident light photoconversion efficiency (IPCE) was nearly 2.5–4.5 times higher than that on 0D TNP/Ti disk (Fig. 7 (d)), all of which could eventually benefit the observed photocatalytic activity and efficiency (Fig. 6 and Table 2).

On the other hand, the findings have been similarly reported for a carbon nanotubes/titanium dioxide ($CNTs/TiO_2$) composite prepared by a novel surfactant wrapping sol–gel method, on which a significant photo-activity enhancement has been successfully observed for the first time [40,41]. In principle, in both systems of $CNTs/TiO_2$ and TNT/Ti, the CNT and the TNT act as a electron sinks, and the observed photo-activity enhancement on these two composites should be mainly attributed to the capability of the CNTs and TNTs as well as the applied potential to facilitate the separation, transfer and utilization of the photo-generated electron/hole pairs at the $CNTs–TiO_2$ and $Ti–TiO_2$ interfaces, respectively. Moreover, further detailed discussions have been professionally carried out [40].

4. Conclusions

The current effort of TNT–TBPC system was experimentally validated a much more effective removal efficiency of RB substrate

Table 2
The kinetic constants in TNT- and TNP–TBPC systems at ω of 30 rpm.

RB concentration (mg/L)	Kinetic Constants[a] k_{app} (min^{-1})	Regression coefficients R^2	Kinetic Constants[b] k_{app} (min^{-1})	Regression coefficients R^2
10	0.0139	0.9206	0.0094	0.9424
20	0.0119	0.9915	0.0080	0.9311
30	0.0102	0.9466	0.0058	0.9385
50	0.0146	0.9451	0.0078	0.9497
80	0.0113	0.9631	0.0054	0.9854
100	0.0079	0.9780	0.0044	0.9688

[a] TNT–TBPC.
[b] TNP–TBPC.

than the conventional counterpart. Following conclusions could be drawn:

1) The prepared 1D TNTs on 38 cm^2 were 14.9 μm long with an average pore size of 75 nm and a wall thickness of 17 nm, but a relatively low morphological quality was also observed.

2) An excellent RB removal efficiency of nearly 90% and a COD removal efficiency of 56% were obtained within 3 h photocatalytic treatment in TNT–TBPC system.

3) An improved RB removal efficiency of nearly 30–55% was observed in TPC than BPC, which indicated that in TNT–TBPC system, the main photo-driven degradation and mineralization processes occurred on the upper half of rotating disk, in form of TPC.

4) An improved RB removal efficiency of nearly 25–40% was observed in TNT–TBPC than TNP–TBPC system, which indicated the significantly large application potentials for environmental purifications, and could be attributed to the dramatically superior photon efficiency, quantum yield and photocarriers separation, transfer and utilization on the highly ordered, vertically oriented 1D TNT/Ti rotating disk.

Acknowledgments

References

[1] G.K. Mor, K. Shankar, M. Paulose, O.K. Varghese, C.A. Grimes, Enhanced photocleavage of water using titania nanotube-arrays, Nano Lett. 5 (2005) 191–195.

[2] J.H. Park, S. Kim, A.J. Bard, Novel carbon-doped TiO$_2$ nanotube arrays with high aspect ratios for efficient solar water splitting, Nano Lett. 6 (2006) 24–28.

[3] N.A. Hamill, L.R. Weatherley, C. Hardacre, Use of a batch rotating photocatalytic contactor for the degradation of organic pollutants in wastewater, Appl. Catal. B: Environ. 30 (2001) 49–60.

[4] H. Chen, S. Chen, X. Quan, H.T. Yu, H.M. Zhao, Y.B. Zhang, Fabrication of TiO$_2$–Pt coaxial nanotube array schottky structures for enhanced photocatalytic degradation of phenol in aqueous solution, J. Phys. Chem. C 112 (2008) 9285–9290.

[5] K. Shankar, J. Bandara, M. Paulose, H. Wietasch, O.K. Varghese, G.K. Mor, T.J. LaTempa, M. Thelakkat, C.A. Grimes, Highly efficient solar cells using TiO$_2$ nanotube arrays sensitized with a donor-antenna dye, Nano Lett. 8 (2008) 1654–1659.

[6] H.F. Zhuang, C.J. Lin, Y.K. Lai, L. Sun, J. Li, Some critical structure factors of titanium oxide nanotube array in its photocatalytic activity, Environ. Sci. Technol. 41 (2007) 4735–4740.

[7] X. Quan, S.G. Yang, X.L. Ruan, H.M. Zhao, Preparation of titania nanotubes and their environmental applications as electrode, Environ. Sci. Technol. 39 (2005) 3770–3775.

[8] K. Zhu, T.B. Vinzant, N.R. Neale, A.J. Frank, Removing structural disorder from oriented TiO$_2$ nanotube arrays: reducing the dimensionality of transport and recombination in dye-sensitized solar cells, Nano Lett. 7 (2007) 3739–3746.

[9] G.K. Mor, K. Shankar, M. Paulose, O.K. Varghese, C.A. Grimes, Use of highly-ordered TiO$_2$ nanotube arrays in dyesensitized solar cells, Nano Lett. 6 (2006) 215–218.

[10] K. Zhu, N.R. Neale, A. Miedaner, A.J. Frank, Enhanced charge-collection efficiencies and light scattering in dye-sensitized solar cells using oriented TiO$_2$ nanotubes arrays, Nano Lett. 7 (2007) 69–74.

[11] G.K. Mor, K. Shankar, M. Paulose, O.K. Varghese, C.A. Grimes, Enhanced photocleavage of water using titania nanotube arrays, Nano Lett. 5 (2005) 191–195.

[12] D.D. Dionysiou, A.P. Khodadoust, A.M. Kern, M.T. Suidan, I. Baudin, J.M. Laîné, Continuous-system photocatalytic degradation of chlorinated phenols and pesticides in water using a bench-scale TiO$_2$ rotating disk reactor, Appl. Catal. B: Environ. 24 (2000) 139–155.

[13] Z.Y. Liu, X.T. Zhang, S. Nishimoto, M. Jin, D.A. Tryk, T. Murakami, A. Fujishima, Highly ordered TiO$_2$ nanotube arrays with controllable length for photoelectrocatalytic degradation of phenol, J. Phys. Chem. C 112 (2008) 253–259.

[14] A.K. Ray, A.A.C.M. Beenackers, Development of a new photocatalytic reactor for purification, Catal. Today 40 (1998) 73–83.

[15] P.S. Mukherjee, A.K. Ray, Major challenges in the design of a large-scale photocatalytic reactor for water treatment, Chem. Eng. Technol. 22 (1999) 253–260.

[16] L.F. Zhang, W.A. Anderson, Z.S. Zhang, Development and modeling of a rotating disc photocatalytic reactor for wastewater treatment, Chem. Eng. J. 121 (2006) 125–134.

[17] D.D. Dionysiou, G. Balasubramanian, M.T. Suidan, A.P. Khodadoust, I. Baudin, J.M. Laîné, Rotating disk photocatalytic reactor: development, characterization, and evaluation for the destruction of organic pollutants in water, Water Res. 34 (2000) 2927–2940.

[18] D.D. Dionysiou, M.T. Suidan, I. Baudin, J.M. Laîné, Oxidation of organic contaminants in a rotating disk photocatalytic reactor: reaction kinetics in the liquid phase and the role of mass transfer based on the dimensionless Damkohler number, Appl. Catal. B: Environ. 38 (2002) 1–16.

[19] H.V. Parys, E. Tourwé, T. Breugelmans, M. Depauw, J. Deconinck, A. Hubin, Modeling of mass and charge transfer in an inverted rotating disk electrode (IRDE) reactor, J. Electroanal. Chem. 622 (2008) 44–50.

[20] P. Mandin, T. Pauport, P. Fanouillere, D. Lincot, Modeling and numerical simulation of hydrodynamical processes in a confined rotating electrode configuration, J. Electroanal. Chem. 565 (2004) 159–173.

[21] D. Sopchak, B. Miller, Y. Avyigal, R. Kalish, Rotating ring/disk electrode studies of the oxidation of pmethoxyphenol and hydroquinone at boron-doped diamond electrodes, J. Electroanal. Chem. 538–539 (2002) 39–45.

[22] C. Hardacre, E.A. Mullan, D.W. Rooney, J.M. Thompson, Use of a rotating disc reactor to investigate the heterogeneously catalysed oxidation of cinnamyl alcohol in toluene and ionic liquids, J. Catal. 232 (2005) 355–365.

[23] R.A. Damodar, T. Swaminathan, Performance evaluation of a continuous flow immobilized rotating tube photocatalytic reactor (IRTPR) immobilized with TiO$_2$ catalyst for azo dye degradation, Chem. Eng. J. 144 (2008) 59–66.

[24] D.D. Dionysiou, A.A. Burbano, M.T. Suidan, I. Baudin, J.M. Laîné, Effect of oxygen in a thin-film rotating disk photocatalytic reactor, Environ. Sci. Technol. 36 (2002) 3834–3843.

[25] L.F. Zhang, T. Kanki, N. Sano, A. Toyoda, Photocatalytic degradation of organic compounds in aqueous solution by a TiO$_2$-coated rotating-drum reactor using solar light, Sol. Energy 70 (2001) 331–337.

[26] Y.L. Xu, Y. He, X.D. Cao, D.J. Zhong, J.P. Jia, TNT/Ti rotating disk photoelectro-catalytic (PEC) reactor: a combination of highly effective thin-film PEC and conventional PEC processes on a single electrode, Environ. Sci. Technol. 42 (2008) 2612–2617.

[27] D.D. Dionysiou, M.T. Suidan, I. Baudin, J.M. Laîné, Effect of hydrogen peroxide on the destruction of organic contaminants-synergism and inhibition in a continuous-system photocatalytic reactor, Appl. Catal. B: Environ. 50 (2004) 259–269.

[28] A.Y. Zhang, M.H. Zhou, L. Liu, W. Wang, Y.L. Jiao, Q.X. Zhou, A novel photoelectrocatalytic system for organic contaminant degradation on a TiO$_2$ nanotube (TNT)/Ti electrode, Electrochim. Acta 55 (2010) 5091–5099.

[29] C.C. Chen, H.W. Chung, C.H. Chen, H.P. Lu, C.M. Lan, S.F. Chen, L.Y. Luo, C.S. Hung, E.W.G. Diau, Fabrication and characterization of anodic titanium oxide nanotube arrays of controlled length for highly efficient dye-sensitized solar cells, J. Phys. Chem. C 112 (2008) 19151–19157.

[30] F.I. Marin, M.A. Hamstra, D. Vanmaekelbergh, Greatly enhanced sub-bandgap photocurrent in porous GaP photoanodes, J. Electrochem. Soc. 143 (1996) 1137–1142.

[31] G.K. Mor, O.K. Varghese, M. Paulose, N. Mukherjee, C.A. Grimes, Fabrication of tapered, conical-shaped titania nanotubes, J. Mater. Res. 18 (2003) 2588–2593.

[32] G.K. Mor, O.K. Varghese, M. Paulose, K.G. Ong, C.A. Grimes, Fabrication of hydrogen sensors with transparent titanium oxide nanotube-array thin films as sensing elements, Thin Solid Films 496 (2006) 42–48.

[33] O.K. Varghese, M. Paulose, K. Shankar, G. Mor, C.A. Grimes, Water-photolysis properties of micron-length highly-ordered titania nanotube-arrays, J. Nanosci. Nanotechnol. 5 (2005) 1158–1165.

[34] S.K. Mohapatra, K.S. Raja, M. Misra, V.K. Mahajan, M. Ahmadian, Synthesis of self-organized mixed oxide nanotubes by sonoelectrochemical anodization of Ti–8Mn alloy, Electrochim. Acta 53 (2007) 590–597.

[35] K. Shankar, G.K. Mor, A. Fitzgerald, C.A. Grimes, Cation effect on the electrochemical formation of very high aspect ratio TiO$_2$ nanotube arrays in formamide-water mixtures, J. Phys. Chem. C 111 (2007) 21–26.

[36] M. Paulose, L. Peng, K.C. Popat, O.K. Varghese, T.J. LaTempa, N.Z. Bao, T.A. Desaic, C.A. Grimes, Fabrication of mechanically robust, large area, polycrystalline nanotubular/porous TiO$_2$ membranes, J. Membr. Sci. 319 (2008) 199–205.

[37] X. Zhao, Y.F. Zhu, Synergetic degradation of Rhodamine B at a porous ZnWO$_4$ film electrode by combined electro-oxidation and photocatalysis, Environ. Sci. Technol. 40 (2006) 3367–3372.

[38] J. Georges, Deviation from Beer's law due to dimerization equilibria: theoretical comparison of absorbance, fluorescence and thermal lens measurements, Spectrochim. Acta A 51 (1995) 985–994.

[39] Q. Zheng, B.X. Zhou, J. Bai, L.H. Li, Z.J. Jin, J.L. Zhang, J.H. Li, Y.B. Liu, W.M. Cai, X.Y. Zhu, Self-organized TiO$_2$ nanotube array sensor for the determination of chemical oxygen demand, Adv. Mater. 20 (2008) 1044–1049.

[40] B. Gao, C. Peng, G.Z. Chen, G. Li Puma, Photo-electro-catalysis enhancement on carbon nanotubes/titanium dioxide (CNTs/TiO$_2$) composite prepared by a novel surfactant wrapping sol-gel method, Appl. Catal. B: Environ. 85 (2008) 17–23.

[41] B. Gao, G.Z. Chen, G. Li Puma, Carbon nanotubes/titanium dioxide (CNTs/TiO$_2$) nanocomposites prepared by conventional and novel surfactant wrapping sol–gel methods exhibiting enhanced photocatalytic activity, Appl. Catal. B: Environ. 89 (2009) 503–509.